Monodisperse Molybdenum Nanoparticles as Highly Efficient Electrocatalysts for Li-S Batteries

Yuping Liu,[1,2] Atasi Chatterjee,[1,4] Pascal Rusch,[2,3] Chuanqiang Wu,[5] Pengfei Nan,[5] Manhua Peng,[1,2] Frederik Bettels,[1,2] Taoran Li,[1,2] Chenxi Ma,[1,2] Chaofeng Zhang,[5] Binghui Ge,[5] Nadja C. Bigall,[2,3,6] Herbert Pfnür,[1,2] Fei Ding,[1,2] and Lin Zhang*[1,2]

[1]Institute of Solid State Physics, [2]Laboratory of Nano and Quantum Engineering (LNQE), [3]Institute of Physical Chemistry and Electrochemistry, [6]Cluster of Excellence PhoenixD (Photonics, Optics, and Engineering – Innovation Across Disciplines), Leibniz University Hannover, 30167 Hannover, Germany

[4]2.6 Electrical Quantum Metrology, Physikalisch-Technische Bundesanstalt (PTB), 38116 Braunschweig, Germany

[5]Information Materials and Intelligent Sensing Laboratory of Anhui Province, Key Laboratory of Structure and Functional Regulation of Hybrid Materials of Ministry of Education, Institutes of Physical Science and Information Technology, Anhui University, Hefei 230601, China

*Corresponding Authors: lin.zhang@fkp.uni-hannover.de

Abstract: Lithium-sulfur (Li-S) batteries have attracted widespread attention due to their high theoretical energy density. However, their practical application is still hindered by the shuttle effect and the sluggish conversion of lithium polysulfides (LiPSs). Herein, monodisperse molybdenum (Mo) nanoparticles embedded onto nitrogen-doped graphene (Mo@N-G) were developed and used as a highly efficient electrocatalyst to enhance LiPS conversion. The weight ratio of the electrocatalyst in the catalyst/sulfur cathode is only 9%. The unfilled d orbitals of oxidized Mo can attract the electrons of LiPS anions and form Mo-S bonds during the electrochemical process, thus facilitating fast conversion of LiPSs. Li-S batteries based on the Mo@N-G/S cathode can exhibit excellent rate performance, large capacity, and superior cycling stability. Moreover, Mo@N-G also plays an important role in room-temperature (RT)

quasi-solid-state (QSS) Li-S batteries. These interesting findings suggest the great potential of Mo nanoparticles in building high-performance Li-S batteries.

Keywords: *Mo-based compounds*, *monodisperse Mo nanoparticles*, *electrocatalyst*, *Mo-S bond*, *quasi-solid-state*, *Li-S batteries*

Li-S batteries have been generally considered promising candidates for next-generation energy storage systems due to their high theoretical energy density (2600 Wh kg^{-1}), environmental benignity, and low cost.[1-3] Nevertheless, the commercial applications of Li-S batteries are still restrained by significant challenges, such as the dissolution of intermediate lithium polysulfides (LiPSs) into organic electrolytes (known as the "shuttle effect"), corrosion of Li metal, severe fading of capacity, and low Coulombic efficiency (CE).[4-6] In addition, the low conductivity of S and its discharge products (especially Li_2S) leads to sluggish electrochemical reaction kinetics and low S utilization.[7, 8]

Tremendous efforts have been made in recent years. For example, carbonaceous material hosts can physically confine sulfur and thus effectively mitigate the poor electrical conductivity of S and the loss of soluble LiPSs.[9, 10] Nevertheless, the electrochemical performance of these materials is mediocre, due mainly to the poor affinity of nonpolar carbon to the polarized LiPSs. To address this issue, a number of strategies have been developed, including heteroatom doping[11-13] and using metal sulfide, oxide, nitride, and metal-organic framework (MOF) hosts.[14, 15] Although considerable improvements have been achieved, these improvements fail to enhance the intrinsically sluggish reaction kinetics of LiPSs with limited host materials, especially the liquid-solid phase transformation of soluble Li_2S_4 to solid Li_2S (which contributes 75% of the theoretical capacity of the Li-S battery).[16-19]

For decades, Mo-based compounds (*e.g.*, sulfides, carbides, nitrides, phosphides, borides) have been considered promising catalysts in electrochemical water splitting toward the hydrogen evolution reaction (HER).[20, 21] Highly efficient catalyst activities for the HER were

reported, which endorse the potential of Mo-based compounds to replace costly platinum (Pt) catalysts.[20, 21] Recently, Mo-based compounds were also investigated as highly effective catalysts for Li-S batteries; Mo-based compounds can enhance both the reduction of S and the oxidation of Li_2S, trap dissolved LiPSs and promote LiPS redox kinetics. These effects together lead to much improved S utilization, rate performance, and cycling stability of Li-S batteries.[22-25] However, these reported Mo-based catalysts have relatively large sizes and can only provide a limited number of active sites, thus requiring a large amount of catalyst in the S cathode, and the weight ratio of the catalyst in the catalyst/sulfur cathode is more than 40%.[22, 25] In addition to Mo-based catalysts, there are several other promising catalysts for Li-S batteries, such as single atom-[26] and defect-based catalysts.[27] However, to date, no reported catalyst can suppress the growth of Li dendrites in all-solid-state (ASS) or quasi-solid-state (QSS) Li-S batteries[28] Therefore, an ideal host material for sulfur should have excellent conductivity, a large number of active sites for effective LiPS adsorption, highly efficient conversion of LiPSs, a relatively low weight ratio of catalyst in the S cathode, and even the ability to catalyze the conversion of sulfur in ASS or QSS Li-S batteries.

On the other hand, in energy storage applications, there have been a few investigations on Mo_2S-based Li-ion batteries.[29] The lithiation of MoS_2 is believed to first undergo Li^+ intercalation and then the conversion reaction to Mo nanoparticles and Li_2S. After the initial lithiation, the conversion is $S + 2Li^+ + 2e^- \rightarrow Li_2S$. The as-formed Mo nanoparticles can increase the electronic/ionic conductivities, interact strongly with LiPSs *via* the Mo-S bond, and therefore improve the battery performance.[30, 31] Now, the interesting question is whether *pristine* Mo nanoparticles with extremely small sizes (not derived from Mo-based compounds) can be used as highly efficient catalysts for Li-S batteries. If the answer is yes, then the maximal utilization of Mo catalysts *at the atomic scale* will shed light on the development of Li-S batteries.

In this work, we provide evidence that monodisperse Mo nanoparticles (with an average diameter of 1.24 nm and embedded onto nitrogen-doped graphene, Mo@N-G) can be used as a highly efficient catalyst for Li-S batteries. The weight ratio of the Mo@N-G catalyst in the Mo@N-G/S cathode is only 9%. The unfilled d orbitals of oxidized Mo can attract the electrons of LiPS anions and form Mo-S bonds during the electrochemical process, thus facilitating a fast conversion of LiPSs. As a result, the Li-S battery with the Mo@N-G/S composite electrode exhibits excellent catalytic activity, enhanced cycle stability and rate capability. Furthermore, when using the Mo@N-G-coated PVDF-HFP/LiTFSI electrolyte in RT QSS Li-S batteries, the overpotential, specific capacity, and stability are significantly improved to levels that are even comparable with the level of their organic electrolyte-based counterparts.

Results and Discussion

Structural and Morphological Characterization of the Mo@N-G

The Mo@N-G composite was prepared by *in situ* pyrolysis (see experimental section),[32, 33] which is illustrated in Figure 1a. First, dicyandiamide (DICY), glucose, and ammonium molybdate salt solutions were dissolved in deionized water, stirred and heated under the protection of N_2 to form a monodisperse distribution of Mo^+. After freeze-drying, the dicyandiamide was condensed onto the layered graphitic carbon nitride ($g-C_3N_4$) and bonded with the aromatic carbon intermediate (from calcined glucose) at approximately 600 °C. Meanwhile, monodisperse metal (Mo) nanoparticles were trapped in the framework of $g-C_3N_4$. Then, at elevated temperatures, Mo nanoparticles were transferred to the graphene matrix *via* the chemical coupling of the nitrogen lone-pair electrons, accompanied by the thermal decomposition of the $g-C_3N_4$ template. Finally, the monodisperse Mo nanoparticles were completely assembled onto N-doped graphene (900 °C).[32, 34, 35]
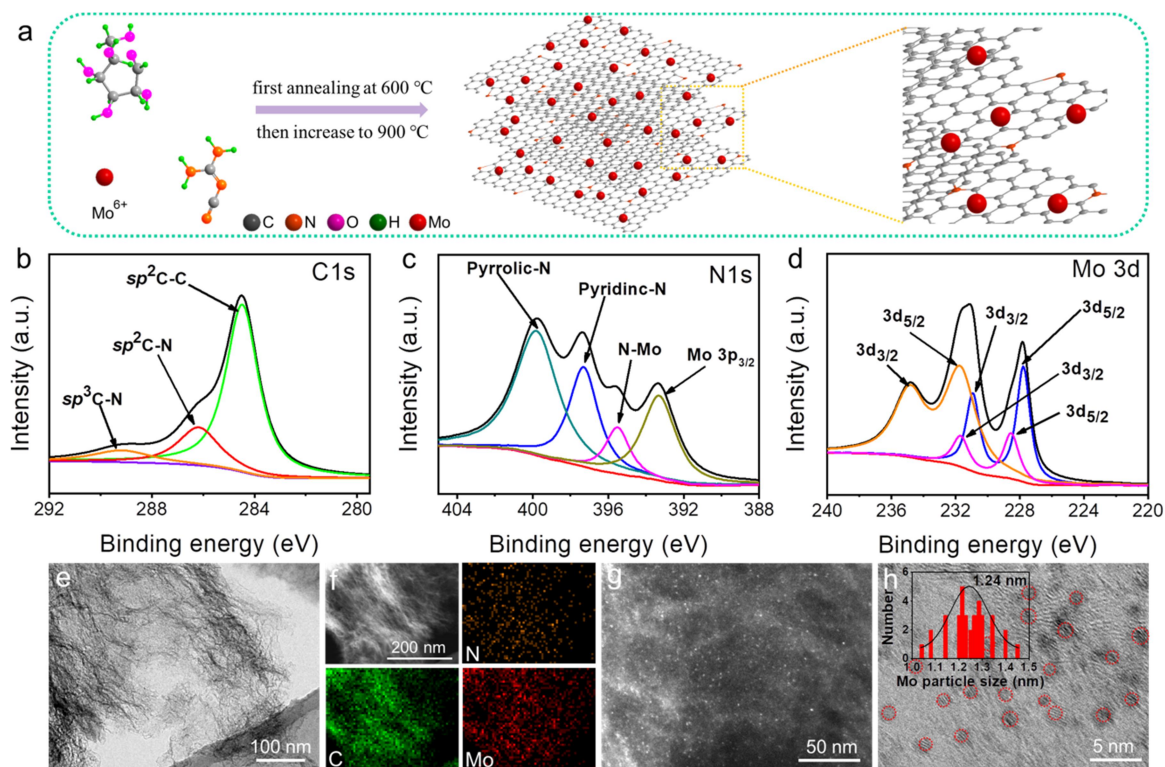
Figure 1. Structural and morphological characterizations of the Mo@N-G composite. (a) Schematic of the synthesis for the Mo@N-G. XPS analysis of the (b) C 1s spectrum, (c) N 1s and Mo $3p_{3/2}$ spectrum, and (d) Mo 3d spectrum. (e) TEM and (f) the corresponding elemental mapping images, (g) the HAADF-STEM image, (h) HRTEM, the inset is the Mo particle size distribution curve.

To gain insight into the compositional and chemical environment of Mo@N-G, high-resolution X-ray photoelectron spectroscopy (XPS) was performed, as shown in Figure 1b-1d. The C 1s spectrum shows a major peak at 284.48 eV, corresponding to the $sp^2C–C$ bond, while the peaks at 286.17 and 289.16 eV correspond to the $sp^2C–N$ and $sp^3C–N$ bonds, respectively.[36] This result confirms the successful nitrogen doping of graphene.[33, 36] Two peaks centered at 397.3 and 399.8 eV in the N 1s spectrum are assigned to pyrrolic-N and pyridinic-N, respectively, and the peak at 395.5 eV can be assigned to the N 1s signal related to the N-Mo bond (Figure 1c).[32, 37, 38] The peak located at 393.3 eV is assigned to Mo $3p_{3/2}$.[39, 40] The Mo 3d XPS shows three intense peaks, which are deconvoluted into three separate doublets with a separation of approximately 3.15 eV. The doublet peaks at 227.78 eV and

230.93 eV (Mo^0), 228.54 eV and 231.69 eV (Mo^{4+}), and 231.71 eV and 234.86 eV (Mo^{6+}) correspond to different oxidation states of Mo $3d_{5/2}$ and Mo $3d_{3/2}$ (from a low oxidation state to a high oxidation state), respectively.[41-43] The variety of Mo valences provides feasibility for further oxidation/reduction. For comparison, the XPS spectrum of the N-G sample is shown in Figure S1a-b, where the C 1s and N 1s data are similar to the data of the Mo@N-G sample but without the presence of the Mo spectrum.

Scanning electron microscopy (SEM) and transmission electron microscopy (TEM) were carried out to study the morphology of Mo@N-G (Figure S2 and Figure 1e-h). The SEM image displays the sheet-like morphology of Mo@N-G, which is similar to graphene. Figure 1e shows the rippled surface of the Mo@N-G nanosheets. The element mapping analysis reveals the homogeneous dispersion of the Mo element throughout the N-doped graphene (Figure 1f). To further reveal the atomic-level structure of Mo@N-G, HAADF-STEM and HRTEM were performed. The HAADF-STEM image shows the uniform distribution of individual Mo nanoparticles (bright spots in Figure 1g) on the graphene nanosheet without any aggregation. HRTEM shows clear lattice stripes and Mo nanoparticles with an average diameter of 1.24 nm, which clearly proves the isolated feature of the Mo nanoparticles (Figure 1h). This feature is crucial in achieving highly efficient catalysis at the atomic scale. Interestingly, the size distribution of the Mo nanoparticles in Mo@N-G is similar to the size distribution of the Mo nanoparticles derived from the Li-MoS$_2$ battery (after lithiation).[44] Furthermore, the specific surface area (SSA) of Mo@N-G was also calculated by N$_2$ adsorption/desorption isotherms, which showed a large value of 489 m^2 g^{-1} (Figure S3). The morphology of the reference N-G sample is similar to the morphology of Mo@N-G but without the presence of Mo nanoparticles (Figure S1c-f).

Electrocatalytic Effect of Mo@N-G toward LiPSs Conversion

6

To show the electrocatalytic effect of Mo@N-G for LiPSs, the kinetics of LiPS conversion reactions were studied. Figure 2a shows the charge/discharge profiles of the Mo@N-G/S, N-G/S, and KB/S electrodes (KB: Ketchen black). The Mo@N-G/S electrode shows a higher capacity contribution from S_8 to Li_2S_4, which illustrates that the Mo nanoparticles have effectively improved the conversion of solid S_8 at the initial stage. Interestingly, the discharge capacity of the N-G/S electrode from the second plateau is much larger than the discharge capacity of the KB/S electrode (from Li_2S_4 to Li_2S) because polar N-doped graphene has a stronger interaction with LiPSs than nonpolar KB, and these results agree with previous studies.[45, 46] The low overpotential demonstrates the high catalytic activity of Mo@N-G toward LiPS conversion.[18] In contrast, the other two electrodes show large voltage hysteresis, especially for the KB/S electrode during deep lithiation/delithiation (between the soluble LiPSs and insoluble Li_2S_2/Li_2S). From the enlarged curves during the charging process (Figure 2b), both the N-G/S and KB/S electrodes exhibit a relatively high potential barrier at approximately 2.29 V (due to the oxidation of Li_2S_2/Li_2S), indicating a sluggish activation process due to the high charge transfer resistance. The Mo@N-G/S electrode, however, shows a distinct voltage jump, suggesting the highest catalytic activity and fastest kinetics among the three samples.[17] This result is extremely important for sulfur utilization and capacity contribution. The improved electrochemical kinetics of Mo@N-G can be attributed mainly to the presence of Mo nanoparticles.
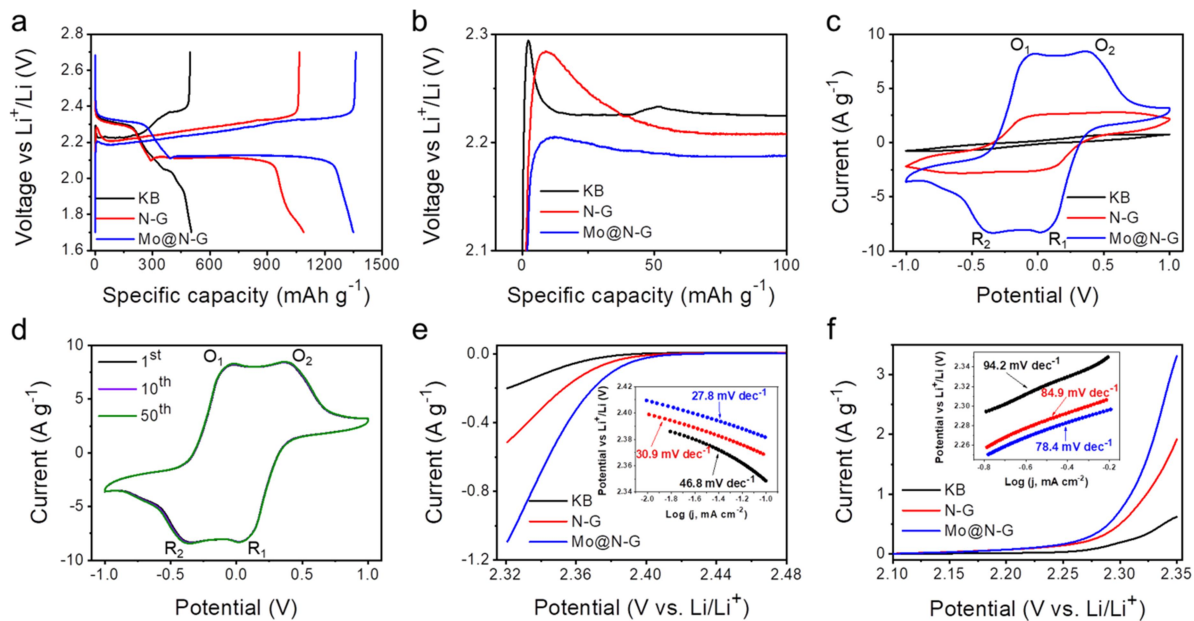
Figure 2. Electrocatalytic effect of Mo@N-G toward LiPS conversion. (a) Charge/discharge profiles of Mo@N-G, N-G and KB electrodes (the second cycle), (b) the overpotentials for conversion between insoluble Li_2S_2/Li_2S and soluble LiPSs (the second cycle), (c) CV curves of symmetric cells with Mo@N-G, N-G, and KB electrodes in electrolytes with 0.2 M Li_2S_6 at 20 mV s^{-1}, (d) CV curves of the Mo@N-G symmetric cell at 20 mV s^{-1} at various cycles. LSV curves of the (e) reduction process and (f) oxidation process for the Li–S cells with Mo@N-G, N-G, and KB electrodes at a scan rate of 0.1 mV s^{-1}. The inset curves are the corresponding Tafel plots.

To further understand the electrocatalytic effect of Mo@N-G for LiPS conversion, cyclic voltammetry (CV) of symmetric cells with identical working and counter electrodes was investigated (with 0.2 M Li_2S_6 electrolyte). For comparison, the electrocatalytic effects of N-G and KB were also tested under the same conditions. As shown in Figure 2c, the CV curve of the Mo@N-G electrode exhibits two pairs of redox peaks at 0.02, -0.34, -0.15, and 0.36 V, respectively. These redox peaks can be attributed to the electrochemical conversion of Li_2S_6. Peaks R_1 and R_2 are the reduction of long-chain LiPSs to short-chain LiPSs and then to Li_2S. In the cathodic scan, the Li_2S was oxidized to the LiPSs and then to S (peaks O_1 and O_2).[47, 48] In sharp contrast, the CV curve of the N-G electrode displays significantly lower current

8

densities, no obvious redox peaks, and a much larger voltage hysteresis. For the KB electrode, the redox peaks are almost invisible. These results are unambiguous evidence for the significant improvement of the electrochemical kinetics of Mo@N-G toward LiPS conversion.

Another finding is that even after 50 cycles, the Mo@N-G electrode still shows well-overlapped CV curves, which further confirms the outstanding stability of the Mo@N-G electrocatalyst (Figure 2d). The Tafel plots were also calculated according to linear sweep voltammetry (LSV) (Figure 2e, f). The cell with the Mo@N-G electrode exhibits the smallest slope during both the cathodic and anodic processes (27.8 mV/dec and 78.8 mV/dec, respectively), indicating the enhanced electrochemical kinetics of the LiPS conversion, which can be clearly attributed to the superior electrocatalytic effect of the Mo nanoparticles in Mo@N-G. These results are consistent with the CV results. Mo@N-G also shows a strong chemical affinity for LiPSs. When Mo@N-G was added to the Li_2S_6 solution, the color of the solution changed from dark yellow to clear after 2 hours, indicating the complete adsorption of Li_2S_6 by Mo@N-G (Figure S4).

Electrochemical Performance of the Mo@N-G/S Cathode (in the Organic Electrolyte)

Encouraged by the superior electrocatalyst effect and chemical affinity of Mo@N-G to LiPSs, the electrochemical performance of Li-S batteries was further evaluated by using Mo@N-G/S cathodes (elemental S was impregnated in the Mo@N-G catalyst through a melt diffusion process under an Ar atmosphere). For comparison, the N-G/S and KB/S electrodes were also prepared under the same conditions. Figure 3a shows the SEM of the Mo@N-G/S electrode after being coated onto the carbon paper current collector. The corresponding element mappings reveal the uniform distribution of N, C, Mo, and S elements in the Mo@N-G/S electrode (Figure 3b). Moreover, TEM characterization was also performed for the Mo@N-G/S cathode, which shows a uniform distribution of these four elements without any obvious accumulation (Figure S5). To confirm the S ratio in the Mo@N-G/S composite,

thermogravimetric analysis (TGA) was carried out, as shown in Figure 3c, which shows an extremely high mass ratio of approximately 91 wt % for S in the cathode. To the best of our knowledge, this value of the S mass ratio is the highest in recent Mo-based compound catalysts in Li-S batteries (Table S1), and some of the values are less than 60%.[22, 25] This high S utilization will significantly improve the energy density of the cell. The electrochemical performance of the Mo@N-G/S electrode was investigated by CV (Figure 3d). The CV curves exhibit two pairs of pronounced reduction and oxidation peaks. The cathodic scan corresponds to the reduction of S to soluble long-chain LiPSs and then to insoluble Li_2S, while the anodic scan corresponds to the oxidation of Li_2S to S, which is consistent with the symmetric cell. The redox peaks almost overlap from the second cycle, indicating the excellent reversibility of the Mo@N-G/S electrode. In sharp contrast, both N-G/S and KB/S electrodes exhibit smaller current densities, and the reduction/oxidation peaks shift significantly, illustrating the sluggish kinetics inside these two electrodes (Figure S6).
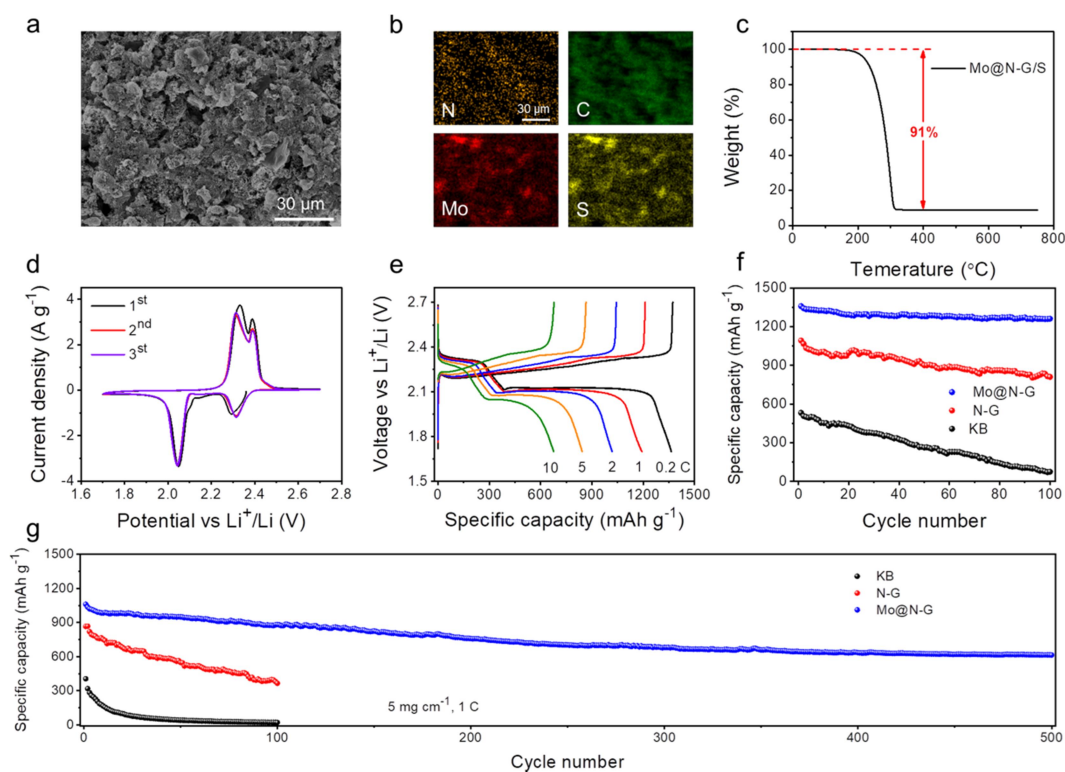

Figure 3. Electrochemical performance of the Mo@N-G/S cathode. (a) SEM and (b) corresponding elemental mapping images of the Mo@N-G/S electrode, (c) TGA curve of the Mo@N-G/S cathode,

(d) CV curves (0.1 mV s^{-1}), (e) charge/discharge profiles of the Li-S battery at different current densities, and (f) cycling performance of the Mo@N-G/S, N-G/S and KB/S electrodes (S loading: 1 mg cm^{-2}, current density: 0.2 C), (g) Long-term stability of Mo@N-G/S, N-G/S, and KB/S electrodes with high S mass loading (5 mg cm^{-2}) under a large current density (1C).

The voltage profiles of the Li-S battery show typical charge/discharge plateaus even under a large current density of 10 C (Figure 3e). In addition, the Mo@N-G/S electrode also delivers excellent rate capability— the discharge capacity is 1365, 1195, 1025, and 842 mAh g^{-1} at 0.2 C, 1 C, 2 C, and 5 C, respectively. Even under a large current density (10 C), the Mo@N-G/S electrode still delivers a large reversible capacity of 676 mAh g^{-1} (Figure S7). The rate performance of the Mo@N-G/S electrode is much better than the rate performance of the N-G/S and KB/S electrodes, and the enhanced kinetics process can be attributed to the Mo electrocatalyst and the good conductivity of Mo@N-G. The enhanced electrochemical kinetics of Mo@N-G/S can also be verified by electrochemical impedance spectroscopy (EIS) measurements. As shown in Figure S8, the Mo@N-G/S electrode displays the lowest charge transfer resistance in its Nyquist plot compared to the N-G/S and KB/S electrodes.

The cycling performance is shown in Figure 3f. The Mo@N-G/S electrode delivers the highest initial discharge capacity of 1359 mAh g^{-1} (corresponding to 81% sulfur utilization) compared to 1092 mAh g^{-1} for the N-G/S electrode (65% sulfur utilization) and 531 mAh g^{-1} for the KB/S electrode (32% sulfur utilization). After 100 cycles, the Mo@N-G/S electrode still maintains 1261 mAh g^{-1}, and the capacity retention is much better than the capacity retention of both the N-G/S and KB/S electrodes. Furthermore, the long-term stability performance of these three cathodes was also measured with a higher sulfur mass loading (5 mg cm^{-2}) and a larger current density (1C). The Mo@N-G/S cathode can still maintain a stable cycling performance (615 mAh g^{-1} after 500 cycles), while the N-G/S and KB/S cathodes show dramatic capacity decay under this stringent condition (Figure 3g). We also

11

noticed another interesting effect. The separator and lithium metal in the after-cycled KB/S cell show a yellow surface, indicating a severe shuttle effect and thus the corrosion of the Li metal (Figure S9). Moreover, the morphology of the Mo@N-G/S and N-G/S electrodes after 50 cycles was also studied by SEM. Impressively, the Mo@N-G/S electrode maintains good integrity without any obvious morphology change. In contrast, the N-G/S electrode shows many holes, due to the weak interaction between the N-G and LiPSs and, consequently, the inverse dissolution of the LiPSs in the electrolyte and the shuttle effect (Figure S10). These results further confirm that Mo@N-G can effectively anchor and catalyze LiPS conversion, thus improving the electrochemical performance of Li-S batteries.

***Ex situ* XPS Study of Cycled Mo@N-G/S Electrodes**

Ex situ XPS analysis of the electrodes (with different depths of discharge/charge, Figure 4a) retrieved from cycled cells was also performed. For the XPS spectrum of Mo (Figure 4b), three separate doublets correspond to Mo $3d_{5/2}$ and Mo $3d_{3/2}$ of Mo@N-G. The Mo^{6+} and Mo^{4+} peaks downshift during discharge compared with the pristine sample, and we also observe a peak at 225 eV attributed to the formation of the Mo-S bond[49, 50] because the unfilled d orbitals of oxidized Mo can attract electrons from LiPS anions and form Mo-S bonds, thus promoting the conversion of LiPSs. Importantly, these doublets of Mo@N-G show reversible upshifts toward their original positions, and the Mo-S bond disappears after the full charge reaches 2.7 V. These results demonstrate the chemical stability of the Mo@N-G catalyst during LiPS conversion.
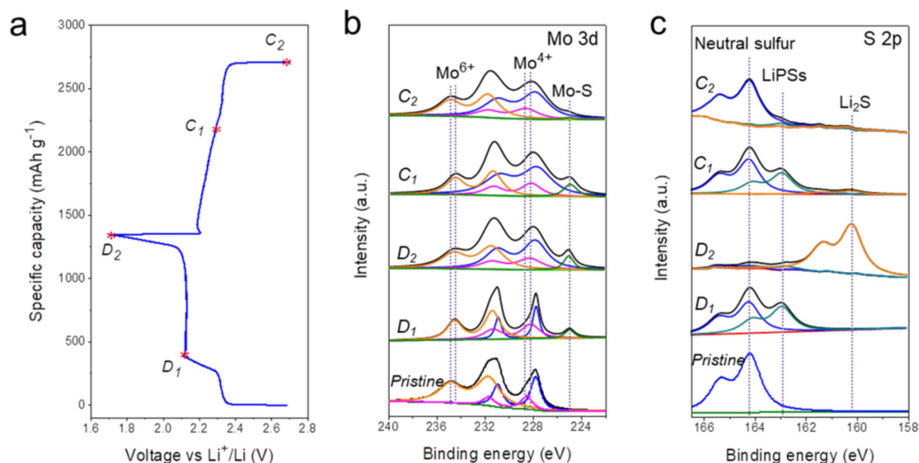
Figure 4. *Ex situ* XPS study of cycled Mo@N-G/S electrodes. (a) Mo@N-G/S electrode at different charge/discharge states, (b) Mo 3d spectrum, and (c) S 2p spectrum at different states.

The S 2p spectra are shown in Figure 4c. For clarity, only the $2p_{3/2}$ component of the S $2p_{3/2}/2p_{1/2}$ spectra in the range of 158–166.5 eV was selected for fitting because the peaks at binding energies over 166.5 eV are dominated by contributions from LiTFSI.[51, 52] During discharge, the characteristic peak of LiPSs appears and is located at 162.9 eV at D_1 = 2.1 V. This peak downshifts (160.2 eV) at D_2 = 1.7 V, which is ascribed to the final products of lithium sulfide.[53] In the subsequent charging process (C_1 = 2.3 V), the characteristic peak of LiPSs is again detected. When charged to C_2 = 2.7 V, the LiPSs were reversibly oxidized to neutral sulfur at 164.2 eV. The evolution of the S 2p spectra proves superior reversibility during the electrochemical process. However, N doping can also improve the electrochemical performance of Li-S batteries by reducing the intrinsic activation barriers during LiPS conversion, as demonstrated in our recent work.[18] Therefore, the chemical affinity and catalytic effect between Mo@N-G and LiPS could be attributed to the synergistic effect of the monodisperse Mo nanoparticles combined with N doping. However, after assembling the Mo nanoparticles, electronic structure analysis reveals that metal-sulfur (Mo-S) pairs dominate the adsorption of sulfur species during the catalysis process.[48, 52, 54] Thus, the improved capacity of the Mo@N-G catalyst is attributed mainly to the Mo nanoparticles.

Mo@N-G Catalyst for RT QSS Li-S Batteries

Inspired by the previous results, the Mo@N-G catalyst was also investigated in RT QSS Li-S batteries (with 60 μm PVDF-HFP/LiTFSI electrolyte, see Experimental Section and Figure S11). Although the QSS electrolyte can inhibit the dissolution of LiPSs and avoid the growth of Li dendrites, the practical application of QSS Li-S batteries is hindered by the high interfacial resistance and instability at high temperatures (usually $\geq 60\ °C$). Here, the Mo@N-G-based QSS Li-S battery exhibits a large specific capacity and small polarization (1193 mAh g^{-1} and 127 mV, respectively), which are even comparable with the specific capacity and polarization of organic electrolyte-based Li-S batteries (Figure 5a, Figure S12). However, the N-G- and KB-based cells delivered only 884 and 441 mAh g^{-1}, with polarizations of 191 and 473 mV, respectively. In addition, the QSS electrolyte without wetting was also tested in Li-S batteries, which shows an electrochemical performance similar to the electrochemical performance of the wetted electrolyte, as shown in Figure S13. To further understand the catalytic effect of Mo@N-G for the QSS electrolyte, the EIS of Li-S cells was measured after three cycles (Figure 5b). Clearly, the Mo@N-G cell has considerably lower resistance than the N-G and KB cells, which indicates the fastest Li-ion diffusion in the Mo@N-G cell.
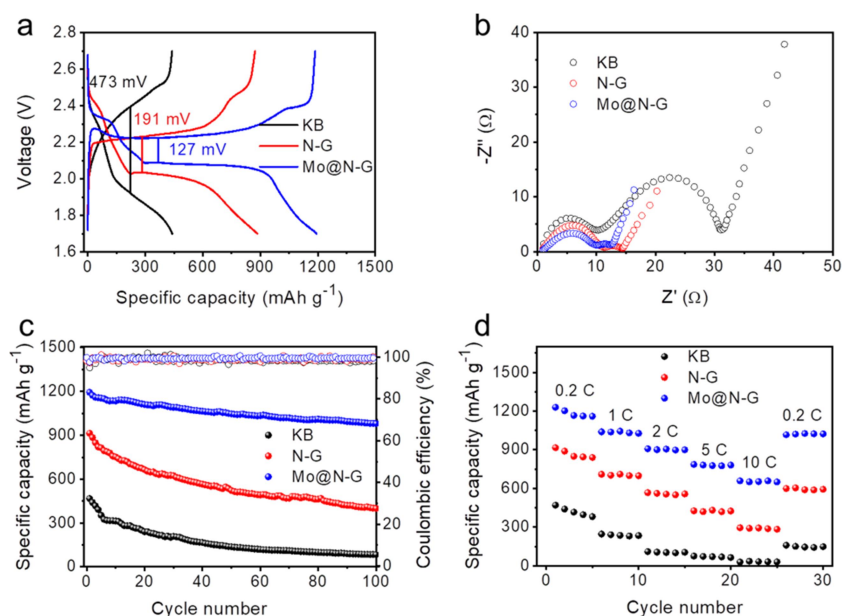

14

Figure 5. Mo@N-G catalyst for the RT QSS Li-S battery. (a) Charge/discharge profiles, (b) Nyquist plots of the impedance spectra, (c) cycling performance (S loading: 1 mg cm^{-2}, current density: 0.2 C), and (d) rate performance.

After 100 cycles, the cell with Mo@N-G still maintains a capacity of 980 mAh g^{-1} with an average CE of 99.5%. In contrast, the cells with N-G and KB showed fast decay and delivered only 399 and 83 mAh g^{-1}, with average CEs of 98.9% and 98.6% after 100 cycles, respectively (Figure 5c). The rate capability also demonstrates the same result. The cell with Mo@N-G exhibits large capacities even under an ultrahigh current density of 10 C (Figure 5d), and these capacities are considerably higher than the capacities of the other two electrodes. In addition, the long-term stability of the cell (with Mo@N-G) under a higher sulfur mass loading (3 mg cm^{-2}) and a larger current density (1 C) was also tested, as shown in Figure S14. Compared with previous PVDF-HFP-based Li-S batteries,[55] the electrochemical performance of this Mo@N-G/S cell shows significant improvement, illustrating the importance of the Mo@N-G catalyst for LiPS conversion in the QSS electrolyte.

Compared with other studies on Mo-based compound catalysts for Li-S batteries, this work further used the Mo-based catalyst on RT QSS Li-S batteries.[56] The well-known problems of large interface resistance and sluggish reaction kinetics have been addressed.[28, 57] The excellent electrochemical performances in this work demonstrate the unobstructed electronic/ionic pathways in the Mo@N-G/S cathode and further confirm the highly efficient catalytic effect of Mo@N-G.

Conclusions

In summary, monodisperse Mo nanoparticles embedded onto N-doped graphene were successfully fabricated. As a highly efficient electrocatalyst, Mo@N-G facilitates fast LiPS conversion and suppresses the shuttle effect. The *ex situ* XPS results demonstrate that the

unfilled *d* orbitals of oxidized Mo can attract the electrons of LiPS anions and form Mo-S bonds, thus promoting the conversion of LiPSs. Therefore, the Li-S battery with Mo@N-G (under a low catalyst ratio) exhibits a large capacity (1359 mAh g^{-1}), superior cycling stability (92.7% capacity retention over 100 cycles), and enhanced reaction kinetics under large current densities (676 mAh g^{-1} under 10 C). Moreover, thanks to the superior electrocatalytic effect and good conductivity of Mo@N-G, the developed RT QSS Li-S batteries exhibit capacity and overpotential that are even comparable with their organic electrolyte-based counterparts. This work provides an exploration of transition metal monodisperse nanoparticle (*e.g.*, W)-based electrocatalysts for high-performance metal-sulfur batteries.

Experimental Section

Materials

Dicyandiamide, glucose, lithium bis(trifluoromethanesulfonyl)imide (LiTFSI) and poly(vinylidene fluoride-cohexafluoropropylene) (PVDF-HFP) were purchased from Sigma–Aldrich. Ammonium molybdate (para) tetrahydrate (99%) was purchased from Alfa-Aesar. All chemical reagents were used without further purification.

Preparation of Mo@N-G and Mo@N-G/S

Then, 5 g dicyandiamide and 0.25 g glucose were dissolved in deionized water, and 2 mL ammonium molybdate salt solution (0.025 M) was added dropwise into the above solution under the protection of N$_2$. The mixture was stirred and heated at 80 °C for 2 h. After cooling and freeze-drying, the precursor was annealed at 600 °C for 2 h and then rose to 900 °C for another 2 h (at a rate of 3 °C/min). As a comparison, nitrogen-doped graphene (N-G) was also prepared using the same method without the addition of the ammonium molybdate salt solution. Mo@N-G/S was prepared by mixing excess sulfur and Mo@N-G and heating at

155 °C under an Ar atmosphere for 12 h, after which the composite was further heated at 200 °C for 2 h. N-G/S and KB/S were prepared using the same method.

Preparation of the QSS Electrolyte

The solid electrolyte was fabricated by mixing LiTFSI and PVDF-HFP (with a mass ratio of 1:1) in N-methyl-2-pyrrolidone (NMP) and drying at 120 °C in a vacuum oven for 24 h (the thickness of this electrolyte was approximately 60 μm). Then, the slurry of Mo@N-G and PVDF-HFP (with a mass ratio of 9:1) in NMP was coated onto the solid electrolyte and dried again, and the areal loading of Mo@N-G was approximately 0.1 mg cm^{-1}. The N-G- and KB-modified solid electrolytes were prepared by the same method.

Materials Characterization

The morphology, microstructure, and composition of the samples were characterized by emission scanning electron microscopy (FE-SEM, JEOL JSM-6700F) and transmission electron microscopy ((HR)TEM, JEOL JEM-2010F) with an energy-dispersive X-ray microanalysis system. XPS analysis was performed with a hemispherical analyzer of 100 mm radius (Leybold Heraeus). The BET specific surface area was obtained using an ASAP2050 instrument (Micromeritics Instrument Corp). Thermogravimetric analysis (Mettler Toledo TGA/DSC 3+) was conducted under an N_2 atmosphere by heating from RT to 750 °C at 5 °C min^{-1}.

Electrochemical Measurements

The sulfur electrodes were prepared using the as-fabricated composites (Mo@NG/S, NG/S, and KB/S) mixed with carbon black and polyvinylidene difluoride (PVDF) at a ratio of 8:1:1 in N-methyl-2-pyrrolidone (NMP) to form a slurry, uniformly coated onto carbon paper and dried in a vacuum oven at 60 °C over 24 h. The electrochemical performances of the

electrodes were evaluated by a CR2032 coin cell, sulfur electrode used as the cathode, with Li foil as the anode, Celgard 2400 membrane as the separator, and 1.0 M LiTFSI in DOL/DME (volume ratio 1:1) with 2 wt % $LiNO_3$ additive as the electrolyte. The electrolyte/sulfur ratio is approximately 4 μl mg^{-1}. For the QSS Li-S batteries, the solid electrolyte was wetted by organic electrolyte and cast on the lithium anode and then assembled with sulfur electrodes. Galvanostatic discharge/charge measurements were performed with a LAND CT 2001A charge/discharge system in the voltage range of 1.7 − 2.7 V. The CV curves were conducted using Metrohm Autolab at a scan rate of 20 mV/s with a voltage range of -1.0 − 1.0 V (symmetric cells), and 0.1 mV s^{-1} for LSV curves with a voltage range of 2.48 – 2.32 V (reduction process) and 2.10 – 2.35 V (oxidation process), respectively. The EIS was measured in the frequency range from 100 kHz to 10 mHz with 10 mV amplitude using the Metrohm Autolab.

Notes

Acknowledgments

Supporting Information

The Supporting Information is available free of charge at……

Table, Figures of XPS, TEM, elemental mapping images, SEM, N_2 adsorption-desorption, digital photograph, CV, rate performance, EIS, charge/discharge profiles, and long-term stability (PDF).

References

(1) Bruce, P. G.; Freunberger, S. A.; Hardwick, L. J.; Tarascon, J. M. Li-O_2 and Li-S Batteries with High Energy Storage. *Nat. Mater.* **2012,** *11*, 19-29.

(2) Yang, Y.; Zheng, G. Y.; Cui, Y. Nanostructured Sulfur Cathodes. *Chem. Soc. Rev.* **2013,** *42*, 3018-3032.

(3) Pang, Q.; Liang, X.; Kwok, C. Y.; Nazar, L. F. Advances in Lithium-Sulfur Batteries Based on Multifunctional Cathodes and Electrolytes. *Nat. Energy* **2016,** *1*, 1-11.

(4) Wang, W. P.; Zhang, J.; Chou, J.; Yin, Y. X.; You, Y.; Xin, S.; Guo, Y. G. Solidifying Cathode-Electrolyte Interface for Lithium-Sulfur Batteries. *Adv. Energy Mater.* **2021,** *11*, 2000791-2000807.

(5) Wu, F. X.; Chu, F. L.; Ferrero, G. A.; Sevilla, M.; Fuertes, A. B.; Borodin, O.; Yu, Y.; Yushin, G. Boosting High-Performance in Lithium-Sulfur Batteries *via* Dilute Electrolyte. *Nano Lett* **2020,** *20*, 5391-5399.

(6) Liu, Y. P.; Zhen, Y. Z.; Li, T. R.; Bettels, F.; He, T.; Peng, M. H.; Liang, Y. C.; Ding, F.; Zhang, L. High-Capacity, Dendrite-Free, and Ultrahigh-Rate Lithium-Metal Anodes Based on Monodisperse N-Doped Hollow Carbon Nanospheres. *Small* **2020,** *16*, 2004770-2004778.

(7) Pang, Q.; Shyamsunder, A.; Narayanan, B.; Kwok, C. Y.; Curtiss, L. A.; Nazar, L. F. Tuning the Electrolyte Network Structure to Invoke Quasi-Solid State Sulfur Conversion and Suppress Lithium Dendrite Formation in Li-S Batteries. *Nat. Energy* **2018,** *3*, 783-791.

(8) Yuan, H.; Peng, H. J.; Li, B. Q.; Xie, J.; Kong, L.; Zhao, M.; Chen, X.; Huang, J. Q.; Zhang, Q. Conductive and Catalytic Triple-Phase Interfaces Enabling Uniform Nucleation in High-Rate Lithium-Sulfur Batteries. *Adv. Energy Mater.* **2019,** *9*, 1802768-1802775.

(9) Jin, S.; Xin, S.; Wang, L. J.; Du, Z. Z.; Cao, L. N.; Chen, J. F.; Kong, X. H.; Gong, M.; Lu, J. L.; Zhu, Y. W.; Ji, H. X.; Ruoff, R. S. Covalently Connected Carbon Nanostructures for Current Collectors in Both the Cathode and Anode of Li-S Batteries. *Adv. Mater.* **2016,** *28*, 9094-9102.

(10) Wu, F. X.; Zhao, E. B.; Gordon, D.; Xiao, Y. R.; Hu, C. C.; Yushin, G. Infiltrated Porous Polymer Sheets as Free-Standing Flexible Lithium-Sulfur Battery Electrodes. *Adv. Mater.* **2016,** *28*, 6365-6371.

(11) Hou, T. Z.; Xu, W. T.; Chen, X.; Peng, H. J.; Huang, J. Q.; Zhang, Q. Lithium Bond Chemistry in Lithium-Sulfur Batteries. *Angew. Chem. Int. Edit.* **2017,** *56*, 8178-8182.

(12) Bao, W. Z.; Liu, L.; Wang, C. Y.; Choi, S.; Wang, D.; Wang, G. X. Facile Synthesis of Crumpled Nitrogen-Doped MXene Nanosheets as a New Sulfur Host for Lithium-Sulfur Batteries. *Adv. Energy Mater.* **2018,** *8*, 1702485-1702495.

(13) Wang, T. Y.; Su, D. W.; Chen, Y.; Yan, K.; Yu, L.; Liu, L.; Zhong, Y. H.; Notten, P. H. L.; Wang, C. Y.; Wang, G. X., Biomimetic 3D Fe/CeO$_2$ Decorated N-Doped Carbon Nanotubes Architectures for High-Performance Lithium-Sulfur Batteries. *Chem. Eng. J.* **2020,** *401*, 126079.

(14) Al Salem, H.; Babu, G.; Rao, C. V.; Arava, L. M. R., Electrocatalytic Polysulfide Traps for Controlling Redox Shuttle Process of Li-S Batteries. *J. Am. Chem. Soc.* **2015,** *137*, 11542-11545.

(15) Chu, Z. H.; Gao, X. C.; Wang, C. Y.; Wang, T. Y.; Wang, G. X., Metal-Organic Frameworks as Separators and Electrolytes for Lithium-Sulfur Batteries. *J. Mater. Chem. A* **2021,** *9*, 7301-7316.

(16) Xu, R.; Lu, J.; Amine, K. Progress in Mechanistic Understanding and Characterization Techniques of Li-S Batteries. *Adv. Energy Mater.* **2015,** *5*, 1500408-1500429.

(17) Zhou, G. M.; Tian, H. Z.; Jin, Y.; Tao, X. Y.; Liu, B. F.; Zhang, R. F.; Seh, Z. W.; Zhuo, D.; Liu, Y. Y.; Sun, J.; Zhao, J.; Zu, C. X.; Wu, D. S.; Zhang, Q. F.; Cui, Y. Catalytic

Oxidation of Li$_2$S on the Surface of Metal Sulfides for Li-S Batteries. *P. Natl. Acad. Sci.* **2017,** *114*, 840-845.

(18) Liu, Y. P.; Ma, S. Y.; Liu, L. F.; Koch, J.; Rosebrock, M.; Li, T. R.; Bettels, F.; He, T.; Pfnür, H.; Bigall, N. C.; Ding, F.; Zhang, L. Nitrogen Doping Improves the Immobilization and Catalytic Effects of Co$_9$S$_8$ in Li-S Batteries. *Adv. Funct. Mater.* **2020,** *30*, 2002462-20022471.

(19) Liu, Y. P.; Barnscheidt, Y.; Peng, M. H.; Bettels, F.; Li, T. R.; He, T.; Ding, F.; Zhang, L., A Biomass-Based Integral Approach Enables Li-S Full Pouch Cells with Exceptional Power Density and Energy Density. *Advanced Science* **2021**, *8*, 2101182-2101189.

(20) Zhuan, Z. C.; Huan, J. Z.; Li, Y.; Zhou, L.; Mai, L. Q. The Holy Grail in Platinum-Free Electrocatalytic Hydrogen Evolution: Molybdenum-Based Catalysts and Recent Advances. *Chemelectrochem* **2019,** *6*, 3570-3589.

(21) Ding, Y.; Fang, L.; Xu, X. X. Polyoxometalate Derived Mo Based Hybrid HER Electrocatalysts with Carbon as Matrix and Their Application in Zn-H$^+$ Battery *J. Clust. Sci.* **2020,** *5*, 1-17.

(22) Li, B. Y.; Su, Q. M.; Yu, L. T.; Zhang, J.; Du, G. H.; Wang, D.; Han, D.; Zhang, M.; Ding, S. K.; Xu, B. S. Tuning the Band Structure of MoS$_2$ *via* Co$_9$S$_8$@MoS$_2$ Core-Shell Structure to Boost Catalytic Activity for Lithium-Sulfur Batteries. *ACS Nano* **2020,** *14*, 17285-17294.

(23) Ma, F.; Wan, Y. Y.; Wang, X. M.; Wang, X. C.; Liang, J. S.; Miao, Z. P.; Wang, T. Y.; Ma, C.; Lu, G.; Han, J. T.; Huang, Y. H.; Li, Q. Bifunctional Atomically Dispersed Mo-N$_2$/C Nanosheets Boost Lithium Sulfide Deposition/Decomposition for Stable Lithium-Sulfur Batteries. *ACS Nano* **2020,** *14*, 10115-10126.

(24) Cheng, Z. B.; Chen, Y. L.; Yang, Y. S.; Zhang, L. J.; Pan, H.; Fan, X.; Xiang, S. C.; Zhang, Z. J. Metallic MoS$_2$ Nanoflowers Decorated Graphene Nanosheet Catalytically Boosts

the Volumetric Capacity and Cycle Life of Lithium-Sulfur Batteries. *Adv. Energy Mater.* **2021,** *11*, 2003718-2003726.

(25) Wang, S. Z.; Feng, S. P.; Liang, J. W.; Su, Q. M.; Zhao, F. P.; Song, H. J.; Zheng, M. H.; Sun, Q.; Song, Z. X.; Jia, X. H.; Yang, J.; Li, Y.; Liao, J. X.; Li, R. Y.; Sun, X. L. Insight into MoS_2-MoN Heterostructure to Accelerate Polysulfide Conversion toward High-Energy-Density Lithium-Sulfur Batteries. *Adv. Energy Mater.* **2021,** *11*, 2003314-2003323.

(26) Wang, Y. C.; Chu, F. L.; Zeng, J.; Wang, Q. J.; Naren, T. Y.; Li, Y. Y.; Cheng, Y.; Lei, Y. P.; Wu, F. X., Single-Atom Catalysts for Fuel Cells and Rechargeable Batteries: Principles, Advances, and Opportunities. *ACS Nano* **2021,** *15*, 210-239.

(27) Shi, Z. X.; Li, M. T.; Sun, J. Y.; Chen, Z. W., Defect Engineering for Expediting Li-S Chemistry: Strategies, Mechanisms, and Perspectives. *Adv. Energy Mater.* **2021**, 2100332-2100357.

(28) Yang, X. F.; Luo, J.; Sun, X. L., Towards High-Performance Solid-State Li-S Batteries: from Fundamental Understanding to Engineering Design. *Chem. Soc. Rev.* **2020,** *49*, 2140-2195.

(29) Wang, T. Y.; Chen, S. Q.; Pang, H.; Xue, H. G.; Yu, Y., MoS_2-Based Nanocomposites for Electrochemical Energy Storage. *Advanced Science* **2017,** *4*, 1600289-1600314.

(30) Zhang, L.; Sun, D.; Kang, J.; Feng, J.; Bechtel, H. A.; Wang, L. W.; Cairns, E. J.; Guo, J. H. Electrochemical Reaction Mechanism of the MoS_2 Electrode in a Lithium-Ion Cell Revealed by *in Situ* and *Operando* X-Ray Absorption Spectroscopy. *Nano Lett* **2018,** *18*, 1466-1475.

(31) Xing, Z. Y.; Tan, G. Q.; Yuan, Y. F.; Wang, B.; Ma, L.; Xie, J.; Li, Z. S.; Wu, T. P.; Ren, Y.; Shahbazian-Yassar, R.; Lu, J.; Ji, X. L.; Chen, Z. W. Consolidating Lithiothermic-Ready Transition Metals for Li_2S-Based Cathodes. *Adv. Mater.* **2020,** *32*, 2002403-2002413.

(32) Liu, D. B.; Wu, C. Q.; Chen, S. M.; Ding, S. Q.; Xie, Y. F.; Wang, C. D.; Wang, T.; Haleem, Y. A.; Rehman, Z. U.; Sang, Y.; Liu, Q.; Zheng, X. S.; Wang, Y.; Ge, B. H.; Xu, H.

X.; Song, L. *In Situ* Trapped High-Density Single Metal Atoms within Graphene: Iron-Containing Hybrids as Representatives for Efficient Oxygen Reduction. *Nano Res.* **2018,** *11*, 2217-2228.

(33) Li, X. H.; Kurasch, S.; Kaiser, U.; Antonietti, M. Synthesis of Monolayer-Patched Graphene from Glucose. *Angew. Chem. Int. Edit.* **2012,** *51*, 9689-9692.

(34) Wang, X. C.; Chen, X. F.; Thomas, A.; Fu, X. Z.; Antonietti, M., Metal-Containing Carbon Nitride Compounds: A New Functional Organic-Metal Hybrid Material. *Adv. Mater.* **2009,** *21*, 1609-1612.

(35) Zhang, G. G.; Huang, C. J.; Wang, X. C., Dispersing Molecular Cobalt in Graphitic Carbon Nitride Frameworks for Photocatalytic Water Oxidation. *Small* **2015,** *11*, 1215-1221.

(36) Chen, X. Y.; Zhang, J.; Ma, S. L.; Hu, H. X.; Zhou, Z. B. Microstructure, Mechanical, and Tribological Properties of CN_x Thin Films Prepared by Reactive Magnetron Sputtering. *Acta. Metall. Sin-Engl.* **2014,** *27*, 31-36.

(37) Li, X. N.; Huang, X.; Xi, S. B.; Miao, S.; Ding, J.; Cai, W. Z.; Liu, S.; Yang, X. L.; Yang, H. B.; Gao, J. J.; Wang, J. H.; Huang, Y. Q.; Zhang, T.; Liu, B. Single Cobalt Atoms Anchored on Porous N-Doped Graphene with Dual Reaction Sites for Efficient Fenton-Like Catalysis. *J. Am. Chem. Soc.* **2018,** *140*, 12469-12475.

(38) Ganesh, R. S.; Silambarasan, K.; Durgadevi, E.; Navaneethan, M.; Ponnusamy, S.; Kong, C. Y.; Muthamizhchelvan, C.; Shimura, Y.; Hayakawa, Y. Metal Sulfide Nanosheet-Nitrogen-Doped Graphene Hybrids as Low-Cost Counter Electrodes for Dye-Sensitized Solar Cells. *Appl. Surf. Sci.* **2019,** *480*, 177-185.

(39) Shi, Z. P.; Nie, K. Q.; Shao, Z. J.; Gao, B. X.; Lin, H. L.; Zhang, H. B.; Liu, B. L.; Wang, Y. X.; Zhang, Y. H.; Sun, X. H.; Cao, X. M.; Hu, P.; Gao, Q. S.; Tang, Y. Phosphorus-Mo_2C@Carbon Nanowires toward Efficient Electrochemical Hydrogen Evolution: Composition, Structural and Electronic Regulation. *Energy Environ. Sci.* **2017,** *10*, 1262-1271.

(40) Wu, C.; Liu, D.; Li, H.; Li, J. H. Molybdenum Carbide-Decorated Metallic Cobalt@Nitrogen-Doped Carbon Polyhedrons for Enhanced Electrocatalytic Hydrogen Evolution. *Small* **2018,** *14*, 1704227-1704236.

(41) Kumar, P.; Singh, M.; Reddy, G. B. Oxidation of Core-Shell MoO_2-MoS_2 Nanoflakes in Different O_2 Ambience. *Mater. Res. Express* **2017,** *4*, 036405.

(42) Zhang, L. N.; Wu, L. L.; Li, J.; Lei, J. L. Electrodeposition of Amorphous Molybdenum Sulfide Thin Film for Electrochemical Hydrogen Evolution Reaction. *BMC Chem.* **2019,** *13*, 1-9.

(43) Syari'ati, A.; Kumar, S.; Zahid, A.; El Yumin, A. A.; Ye, J. T.; Rudolf, P. Photoemission Spectroscopy Study of Structural Defects in Molybdenum Disulfide (MoS_2) Grown by Chemical Vapor Deposition (CVD). *Chem. Commun.* **2019,** *55*, 10384-10387.

(44) Yu, S. H.; Zachman, M. J.; Kang, K.; Gao, H.; Huang, X.; DiSalvo, F. J.; Park, J.; Kourkoutis, L. F.; Abruna, H. D. Atomic-Scale Visualization of Electrochemical Lithiation Processes in Monolayer MoS_2 by Cryogenic Electron Microscopy. *Adv. Energy Mater.* **2019,** *9*, 1902773-1902780.

(45) Pang, Q.; Tang, J. T.; Huang, H.; Liang, X.; Hart, C.; Tam, K. C.; Nazar, L. F. A Nitrogen and Sulfur Dual-Doped Carbon Derived from Polyrhodanine@Cellulose for Advanced Lithium-Sulfur Batteries. *Adv. Mater.* **2015,** *27*, 6021-6028.

(46) Sun, J. H.; Hwang, J. Y.; Jankowski, P.; Xiao, L. H.; Sanchez, J. S.; Xia, Z. Y.; Lee, S.; Talyzin, A. V.; Matic, A.; Palermo, V.; Sun, Y. K.; Agostini, M. Critical Role of Functional Groups Containing N, S, and O on Graphene Surface for Stable and Fast Charging Li-S Batteries. *Small* **2021,** 2007242-2007251.

(47) Lin, H. B.; Yang, L. Q.; Jiang, X.; Li, G. C.; Zhang, T. R.; Yao, Q. F.; Zheng, G. W.; Lee, J. Y. Electrocatalysis of Polysulfide Conversion by Sulfur-Deficient MoS_2 Nanoflakes for Lithium-Sulfur Batteries. *Energy Environ. Sci.* **2017,** *10*, 1476-1486.

(48) Du, Z. Z.; Chen, X. J.; Hu, W.; Chuang, C. H.; Xie, S.; Hu, A. J.; Yan, W. S.; Kong, X. H.; Wu, X. J.; Ji, H. X.; Wan, L. J. Cobalt in Nitrogen-Doped Graphene as Single-Atom Catalyst for High-Sulfur Content Lithium-Sulfur Batteries *J. Am. Chem. Soc.* **2019,** *141*, 3977-3985.

(49) Zheng, Z. L.; Yu, L.; Gao, M.; Chen, X. Y.; Zhou, W.; Ma, C.; Wu, L. H.; Zhu, J. F.; Meng, X. Y.; Hu, J. T.; Tu, Y. C.; Wu, S. S.; Mao, J.; Tian, Z. Q.; Deng, D. H. Boosting Hydrogen Evolution on MoS_2 *via* Co-Confining Selenium in Surface and Cobalt in Inner Layer. *Nat. Commun.* **2020,** *11*, 1-10..

(50) Anjum, M. A. R.; Jeong, H. Y.; Lee, M. H.; Shin, H. S.; Lee, J. S. Efficient Hydrogen Evolution Reaction Catalysis in Alkaline Media by All-in-One MoS_2 with Multifunctional Active Sites. *Adv. Mater.* **2018,** *30*, 1707105-1707113.

(51) Nandasiri, M. I.; Camacho-Forero, L. E.; Schwarz, A. M.; Shutthanandan, V.; Thevuthasan, S.; Balbuena, P. B.; Mueller, K. T.; Murugesan, V. *In Situ* Chemical Imaging of Solid-Electrolyte Interphase Layer Evolution in Li-S Batteries. *Chem. Mater.* **2017,** *29*, 4728-4737.

(52) Zhang, L. L.; Liu, D. B.; Muhammad, Z.; Wan, F.; Xie, W.; Wang, Y. J.; Song, L.; Niu, Z. Q.; Chen, J. Single Nickel Atoms on Nitrogen-Doped Graphene Enabling Enhanced Kinetics of Lithium-Sulfur Batteries. *Adv. Mater.* **2019,** *31*, 1903955-1903963.

(53) Fang, R. Y.; Xu, H. H.; Xu, B. Y.; Li, X. Y.; Li, Y. T.; Goodenough, J. B. Reaction Mechanism Optimization of Solid-State Li-S Batteries with a PEO-Based Electrolyte. *Adv. Funct. Mater.* **2020,** *31*, 2001812-2001818.

(54) Han, X.; Zhang, Z. Y.; Xu, X. F., Single-Atom Catalysts Supported on N-Doped Graphene toward Fast Kinetics in Li-S Batteries: A Theoretical Study. *J. Mater. Chem. A* **2021,** *9*, 12225-12235.

(55) Shanthi, P. M.; Hanumantha, P. J.; Albuquerque, T.; Gattu, B.; Kumta, P. N. Novel Composite Polymer Electrolytes of PVdF-HFP Derived by Electrospinning with Enhanced

Li-Ion Conductivities for Rechargeable Lithium-Sulfur Batteries. *ACS Appl. Energy Mater.* **2018,** *1*, 483-494.

(56) Wang, F. F.; Li, J.; Zhao, J.; Yang, Y. X.; Su, C. L.; Zhong, Y. L.; Yang, Q. H.; Lu, J. Single-Atom Electrocatalysts for Lithium-Sulfur Batteries: Progress, Opportunities, and Challenges. *ACS Mater. Lett.* **2020,** *2*, 1450-1463.

(57) Li, S. L.; Zhang, W. F.; Zheng, J. F.; Lv, M. Y.; Song, H. Y.; Du, L. Inhibition of Polysulfide Shuttles in Li-S Batteries: Modified Separators and Solid-State Electrolytes. *Adv. Energy Mater.* **2020,** *11*, 2000779-2000802.

TOC